**Technical report no. 700/2023**

# Processing of samples from corrosion experiments – Corrosion products 2

Authors: Jan Stoulil et al.

**Prague, 2023**

SÚRAO

**REPORT NAME:** Processing of samples from corrosion experiments – Corrosion products 2

**PROJECT NAME:** Processing of samples from corrosion experiments – Corrosion products 2

**PROJECT IDENTIFICATION:** Final Report

**CONTRACT NO.:** SO2023-002

**AUTHORS:** Stoulil J.[1], Mukhtar S. [1], Lhotka M. [1], Bureš R. [1], Kašpar V. [2], Šachlová Š.[2], Dobrev D.[2], Večerník P.[2], Zuna M.[2], Němeček J.[3], Němeček J.[3]

VŠCHT Praha[1], ÚJV Řež[2], FSv ČVUT[3]

**BIBLIOGRAPHIC RECORD:** Stoulil J. Et al. (2023): Processing of samples from corrosion experiments – Corrosion products 2, SÚRAO technical report TZ 700/2022.

| | |
|---|---|
| **Michaela Matulová** | **Jan Stoulil** |
| Project Manager (SÚRAO) | Project Manager (VŠCHT Prague) |
| 29 September 2023 | 29 September 2023 |

SÚRAO

## Contents

## List of annexes

## List of abbreviations

| | |
|---|---|
| B75 | commercial name for Rokle B75 bentonite (activated with sodium carbonate) |
| BaM | commercial name for Bentonite and Montmorillonite |
| BET | porosity determination method using the Braunauer-Emmett-Teller gas adsorption isotherm |
| BSE | back-scattered electrons (an SEM imaging method) |
| EDS | energy dispersive X-ray spectroscopy (SEM elemental analysis) |
| MaCoTe | Materials Corrosion Test (international project) |
| SE | secondary electron scanning (an SEM imaging method) |
| SEM | scanning electron microscopy |
| WDP | waste disposal package |
| XRD | X-ray diffraction |

## Abstrakt

V rámci krátkého projektu byly hodnoceny vzorky z dlouhodobých experimentů v podzemních laboratořích (MaCoTe a MockUp) a vzorky z dolu Kiruna, kde jsou v dlouhodobém kontaktu částice železné rudy a jílu (bohatého na smektit). Vzorky byly analyzovány pomocí XRD, SEM/EDS, BET a nanoindentace. Výsledky potvrdily, že pravděpodobně není potřeba brát pro modely životnosti UOS v potaz korozní produkty na bázi (hlinito)křemičitanů železa. Dále byly stanoveny moduly pružnosti sideritu, jako hlavního korozního produktu, které jsou nepřímo úměrné mikropórovitosti.

## Klíčová slova

dlouhodobé expozice, korozní produkty, mechanické vlastnosti

## Abstract

This short project involves the evaluation of samples obtained from long-term experiments conducted in underground laboratories (MaCoTe and MockUp) and samples from the Kiruna mine (Sweden), where particles of iron ore and clay (rich in smectite) have been in long-term contact. The samples were analysed by XRD, SEM/EDS, BET and nanoindentation. The results confirmed that it is probably no need to consider corrosion products based on iron (alumino) silicates for the WDP lifetime models. Furthermore, the elastic moduli of siderite (as the main corrosion product), which are inversely proportional to microporosity, were determinated.

## Keywords

Long-term exposure, corrosion products, mechanical properties

# 1 Introduction and description of the samples

Previously conducted projects have determined that the transport of soluble corrosion products through the bentonite pore system, which is gradually sealed over time by newly emerging solid corrosion products, makes up an important factor in terms of the corrosion attack of the outer shell of the waste disposal package (WDP). The dry density of the compacted bentonite comprises one of the most important factors in this respect (Forman et al. 2021). The study of archaeological analogues has revealed, as another important factor, the cyclical mechanical cracking of the layer of corrosion products and the loss of their protective barrier function (Stoulil et al. 2022). Emerging models of outer casing durability will include the factors mentioned above, as well as the synergistic mechanical failure of the outer casing due to corrosion attack and external pressure.

With concern to the cyclical mechanical cracking of the layer of corrosion products and the increase in the external pressure due to the formation of corrosion products that have a higher volume than the original metal, it will be necessary to determine both the porosity and the mechanical properties of the various corrosion products. This project was, therefore, aimed at the verification of these characteristics and the determination of the composition of the various corrosion products. In addition, the project included an examination of the potential alteration of the bentonite material by iron cations.

The bentonite samples consisted of BaM bentonite with a layer of corrosion products obtained from the MaCoTe project (Zuna et al. 2023) following 7 years of exposure to carbon steel in the Grimsel underground laboratory (Switzerland) and Rokle B75 bentonite obtained from the MockUp Josef project following 10 years of exposure to carbon steel in the Josef underground laboratory (Czech Republic). In the latter case, both bentonite samples with corrosion products and the metal itself with corrosion products firmly adhered to it were available for analysis. A further set of samples were obtained from the Kiruna mine (Sweden); these samples were collected as part of the KINA (Kiruna Natural Analogue) project and were kindly provided by Swiss colleagues from Nagra and Japanese colleagues from NUMO. They consist of three different samples extracted from various locations in the mine, see Fig. 1. All the samples consisted of a mixture of clay and iron ore particles that have been in mutual contact for at least $10^8$ years at a depth of around 1320 m. Since the detailed and comprehensive mineralogical characterisation of the samples obtained from Kiruna had already been completed (Gilg and Andersson 2020), this project omitted this stage of the analysis and concentrated on verifying the potential presence of minor secondary (alumino)silicate phases with iron, which theoretically comprised the final corrosion products of the transformation process (Gondolli et al. 2018).

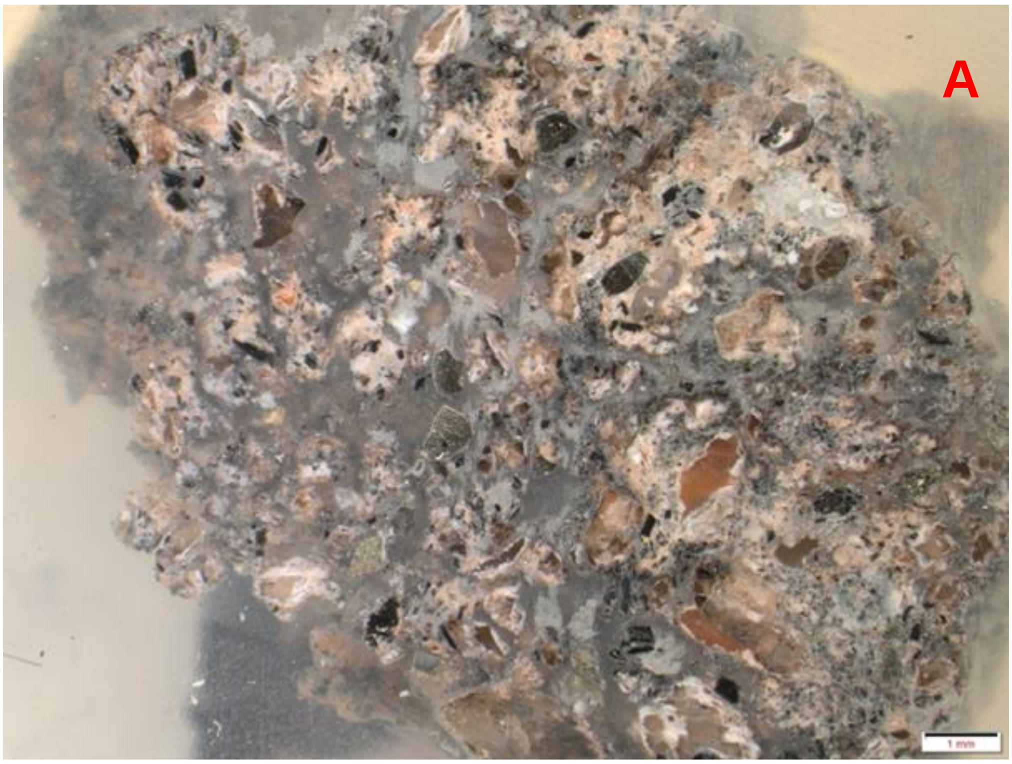
A
1 mm


B
1 mm

*Fig. 1 Images of the Kiruna samples*

# 2 Phase analysis (XRD)

The samples of bentonite with corrosion products (from the MaCoTe and MockUp projects) and the samples obtained from Kiruna were homogenised in friction bowls using a pestle. 2 g of powder from each sample was then used for X-ray diffraction (XRD) analysis. A sample of the surface layer on the metal with adhered corrosion products (MockUp project) was subjected to analysis in the form of one whole item. All the samples were analysed employing an XPert Pro instrument (PANalytical, the Netherlands). The semi-quantitative evaluation of the content of individual phases in such a complicated system was necessarily restricted and is a very rough guide to quantification. However, basically 3 levels of occurrence were evaluated: trace (at the limit of detection, below 5 vol.%), minority (below 20 vol.%) and majority (above 20 vol.%).

Tab. 1 presents a summary of the results on the MaCoTe and MockUp samples. Both samples were found to contain phases that are typical of bentonite, even for samples that were adhered to the metal surface (MockUp). This relates to the early stage of deposition, and, thus, the corrosion products are initially formed in the bentonite pore system. On samples with a deposition time of hundreds of years or more, as in the case of archaeological analogues, do the layers already grow at the interface with the metal, pushing the previously formed layers with bentonite particles further away from the interface (Stoulil et al. 2022). In addition to bentonite particles, the MaCoTe and MockUp samples were also found to contain phases that are likelysecondary corrosion products. The probability was particularly high in this respect concerning magnetite and siderite. The presence of a silicate phase ($Ca_9Fe_6(SiO_4)_4(OH)_{20}$) is debatable; it was not certain whether it is a natural primary phase in the bentonite. The fact that it is a silicate and not an alumino-silicate, however, slighly favours the possibility of a-secondary phase. However, it is important to take into account that Rokle B75 bentonite is activated with sodium carbonate, and the pore solution has a high pH (between 10 and 11). Even if it was a secondary phase, it is not certain that it would be present in natural bentonite. Nevertheless, rarely silicate phases have been observed in corrosion products under natural conditions (Forman et al. 2021).

*Tab. 1 XRD results for the MaCoTe and MockUp samples*

| Phase/Semi-quantitative content | MockUp | MaCoTe |
|---|---|---|
| Montmorillonite | **Majority** | - |
| Silica | **Majority** | Minority |
| Aragonite/Calcite | *Trace* | - |
| Muscovite | - | **Majority** |
| Anatase | *Trace* | *Trace* |

| | | |
|---|---|---|
| Kaolinite | *Trace* | *Trace* |
| Siderite | Minority | Minority |
| Magnetite | Trace | - |
| Ca9Fe6(SiO4)4(OH)20 | Minority | - |

Tab. 2 provides a summary of the results concerning the Kiruna samples. Again, the samples contain phases that are typical for clay, as well as iron ore particles (haematite and magnetite). The origin of the clinochlore phase modified by the presence of a non-negligible number of ferrous cations is debatable. Although it could be a secondary phase formed via the precipitation of dissolved species or directly via the transformation of altered clay particles, the very high content in sample C, in which it comprises the majority phase, appears to be in conflict with this assumption, i.e., the presence of such a high content as a secondary phase is improbable.

*Tab. 2 XRD results for the Kiruna samples*

| **Phase/Semi-quantitative content** | **Kina A** | **Kina B** | **Kina C** |
|---|---|---|---|
| Montmorillonite | Minority | **Majority** | Minority |
| Silica | Minority | *Trace* | Minority |
| Aragonite/Calcite | Minority | Minority | *Trace* |
| Muscovite | Minority | - | - |
| Anatase | *Trace* | - | - |
| Kaolinite | - | - | - |
| Biotite | Minority | *Trace* | - |
| Albite | *Trace* | *Trace* | *Trace* |
| Clinochlore ($Fe^{2+}$) | Minority | *Trace* | **Majority** |
| Haematite | *Trace* | - | *Trace* |
| Magnetite | Minority | *Trace* | Minority |

# 3 Microanalysis

The samples were embedded under reduced pressure conditions in epoxy resin for scanning electron microscope (SEM/EDS) analysis purposes. They were then smoothed using sandpaper and the final smoothing was performed using the finest grade of sandpaper (grain size of P4000). The samples were not polished in case the presence of the diamond paste in the pores would not affect the analysis. The samples were coated with a 0.5 nm layer of gold and analysed using a MIRA II microscope (TESCAN).

Macro images of a vertical section of the MockUp sample are shown in Fig. 2. The width of the altered bentonite layer is around 3.5 mm, while the layer containing precipitated solid corrosion products is around 0.2 mm wide.

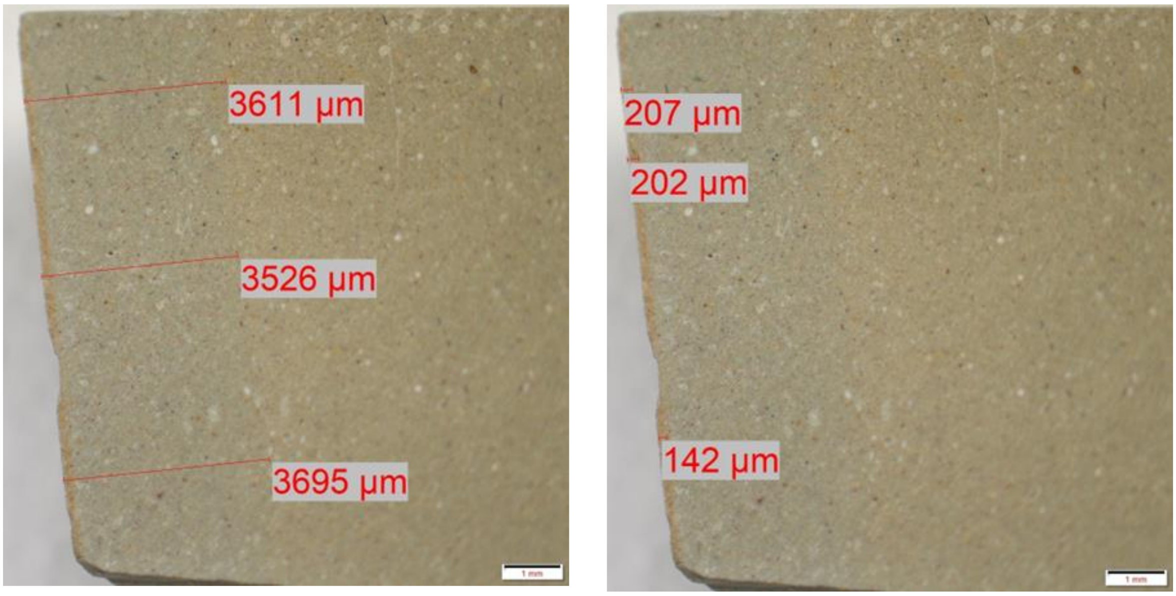

*Fig. 2 Macro images of a vertical section of the MockUp sample: measurements of the altered bentonite layer (left) and the corrosion product layer (right)*

Fig. 3 shows an image of the surface layer of the bentonite with the corrosion products and Fig. 4 presents linear analyses of the Fe content. The concentration of Fe did not indicate an enhanced content in the mixture with the corrosion products nor any indication of a concentration gradient towards the bentonite volume. The concentration of Fe is constant and is the same as that in the unaffected bentonite.

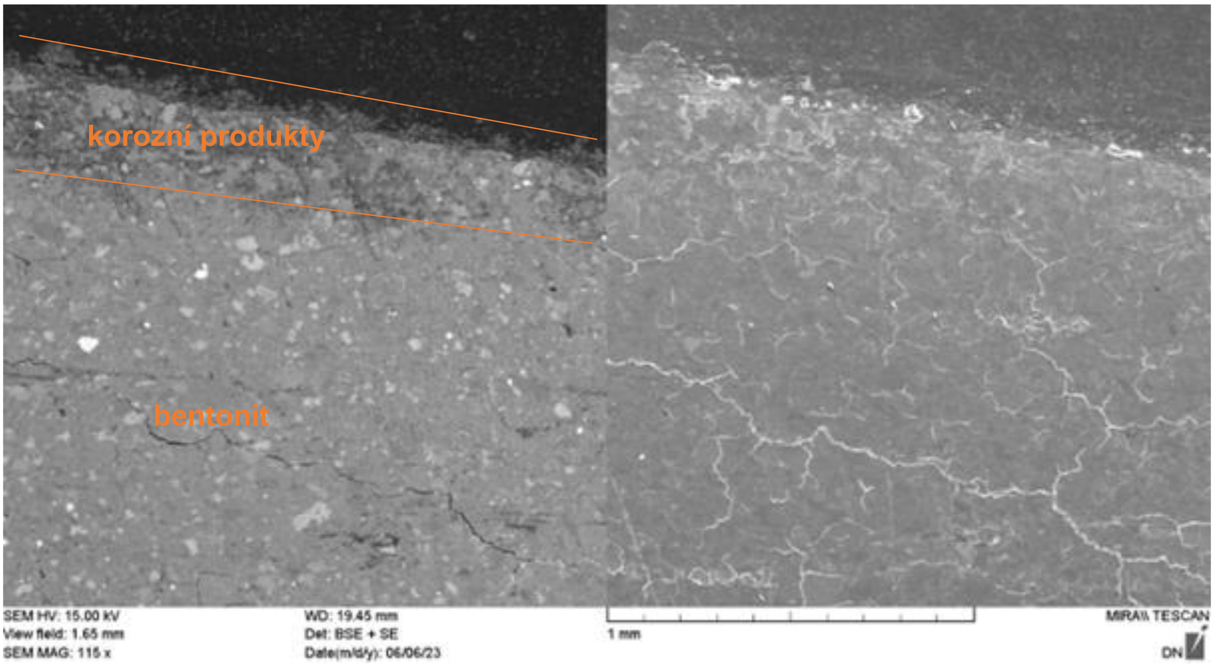

*Fig. 3 SEM images of the MockUp sample: BSE image on the left, SE on the right*

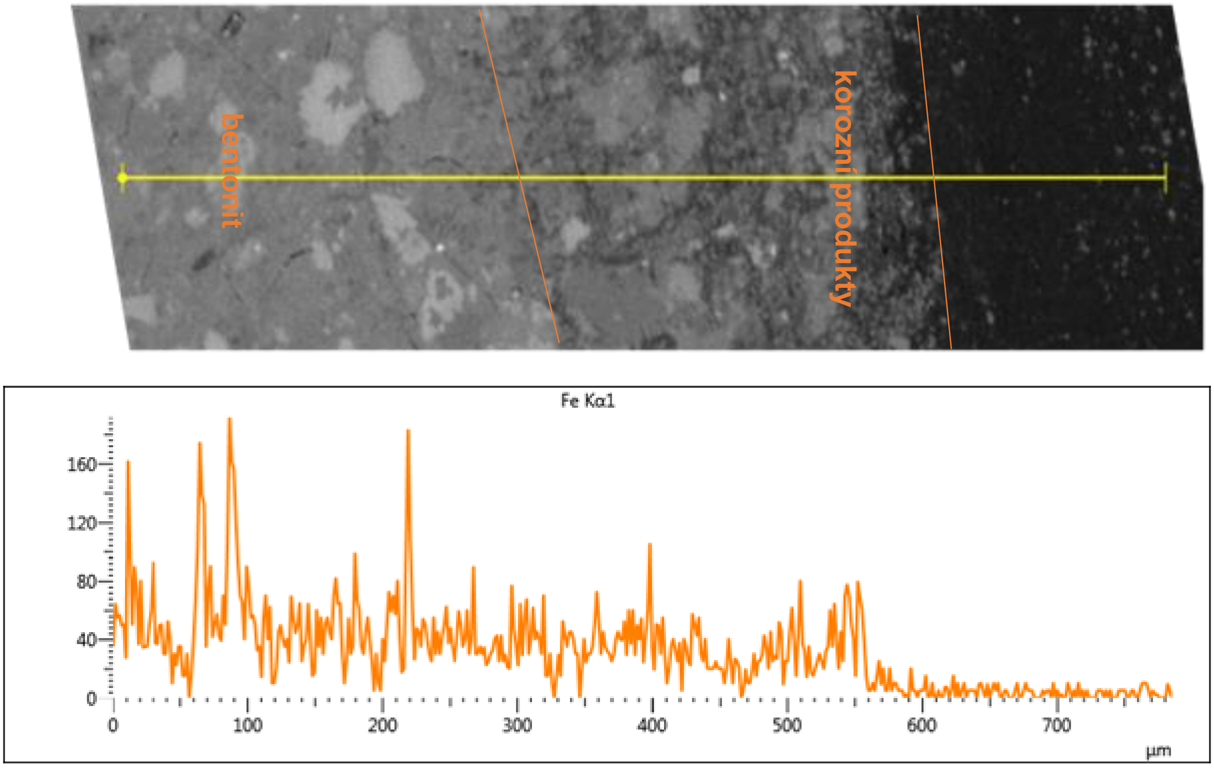

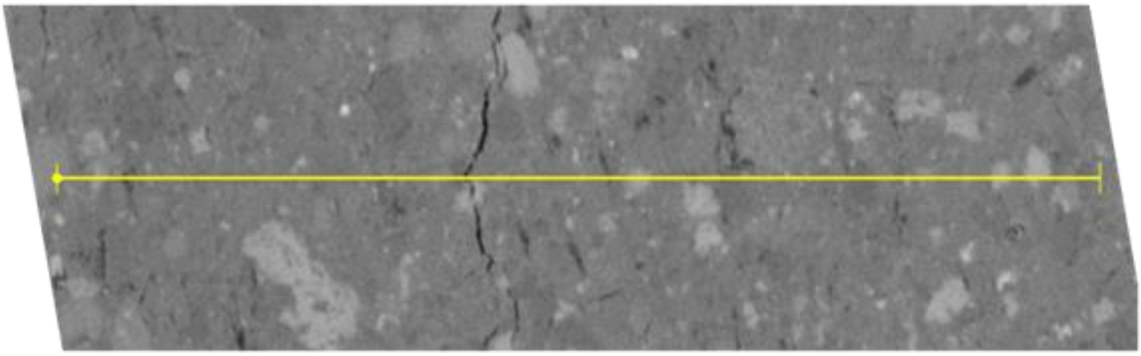

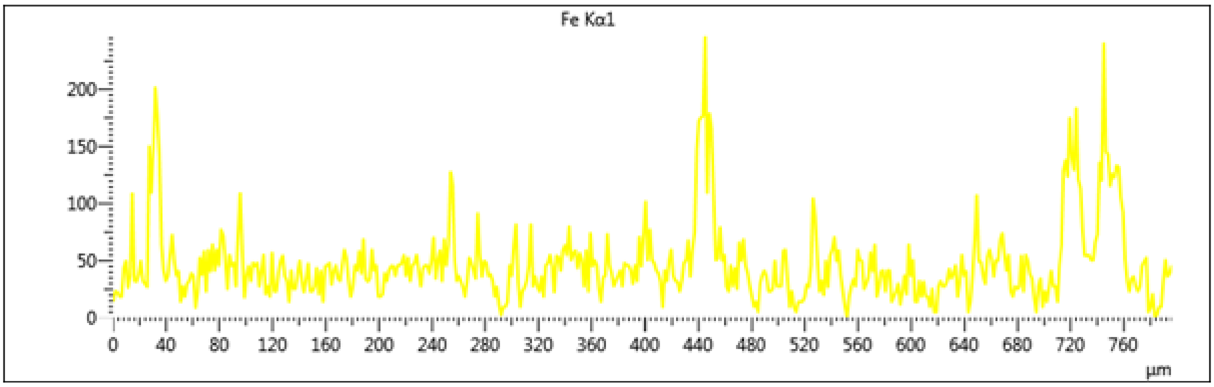
Fe Kα1
0
50
100
150
200
0
40
80
120
160
200
240
280
320
360
400
440
480
520
560
600
640
680
720
760
µm

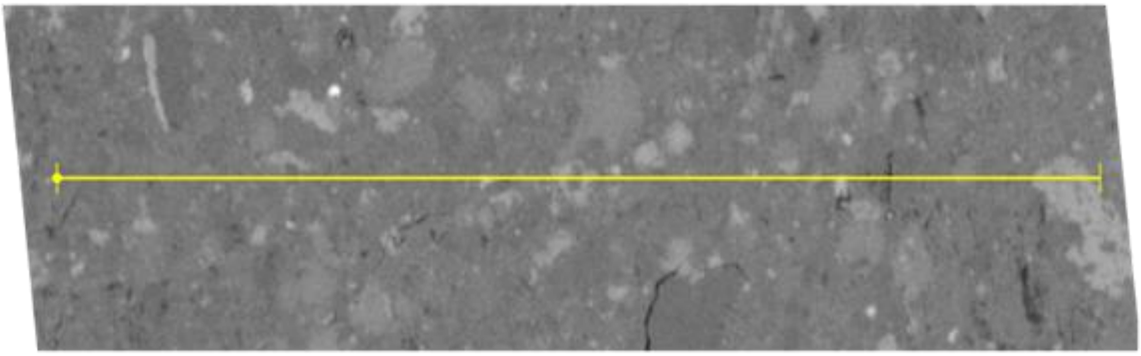

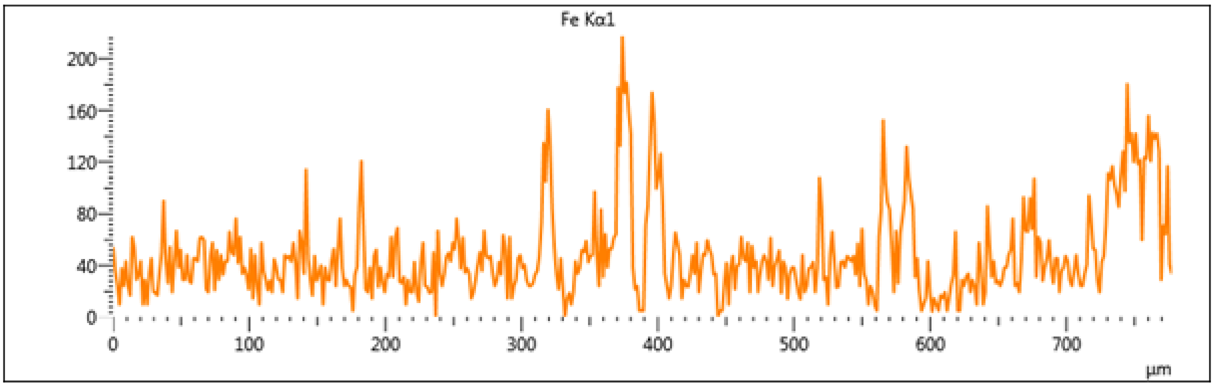
Fe Kα1
0
40
80
120
160
200
0
100
200
300
400
500
600
700
µm

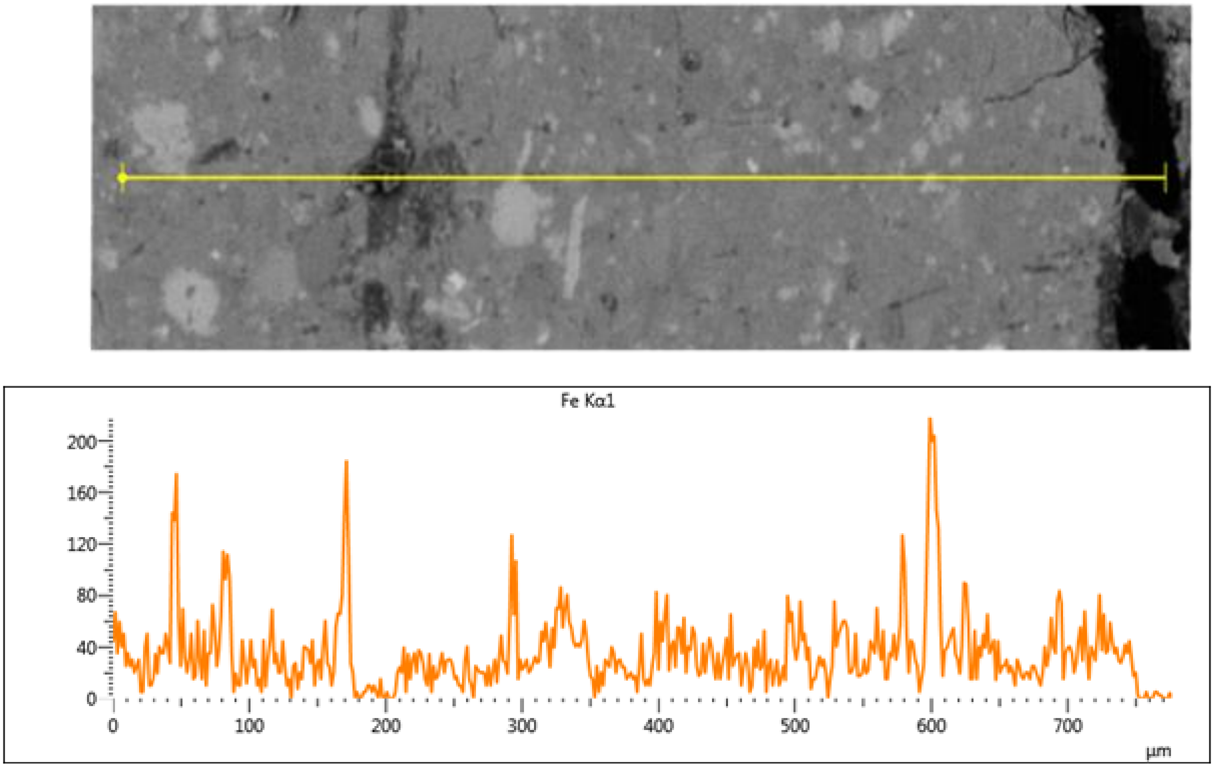

*Fig. 4 MockUp sample - line analyses of the Fe content: from the top: 1. interfaces through the layer with corrosion products, 2. in altered bentonite, 3. interface between the altered/unaltered bentonite, 4. unaltered bentonite.*

A macro image of a perpendicular section of the MaCoTe sample is shown in Fig. 5. The penetration of the alteration of bentonite is similar to that of the MockUp sample, i.e., around 3 mm.

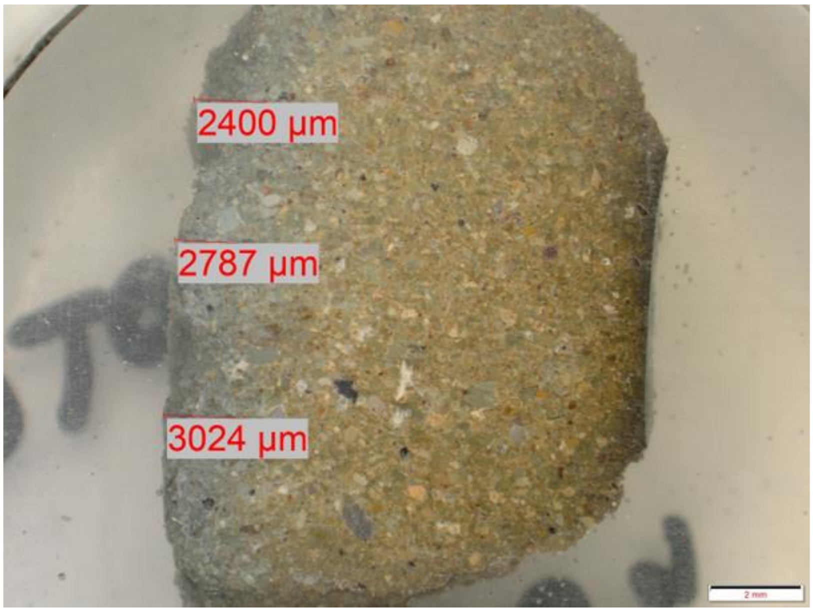

*Fig. 5 Macro image of a perpendicular section of the MaCoTe sample: measurement of the altered bentonite layer*

The SEM images shown in Fig. 6 clearly reveal a layer of corrosion products which is significantly more distinct and, presumably, contains far fewer bentonite particles. A line scan of the Fe concentration through the corrosion product/bentonite interface is shown in Fig. 7. While with respect to the MockUp sample, the Fe signal intensity was similar for both the bentonite and corrosion products, concerning the MaCoTe sample, the intensity for the corrosion products is similar to that of the MockUp sample but significantly higher for the compacted BaM bentonite. However, even in this case, no concentration gradient was observed, and the transitions are very steep. The intensity of the signal is also similar in the deeper parts of the unaltered bentonite (see Fig. 8). Fig. 6 shows that particles with a higher density than the surroundings are visible in the corrosion product layer. One of these lighter particles was analysed in detail (Fig. 9). As shown in the elemental map, the higher carbon content indicates that these particles are siderite.

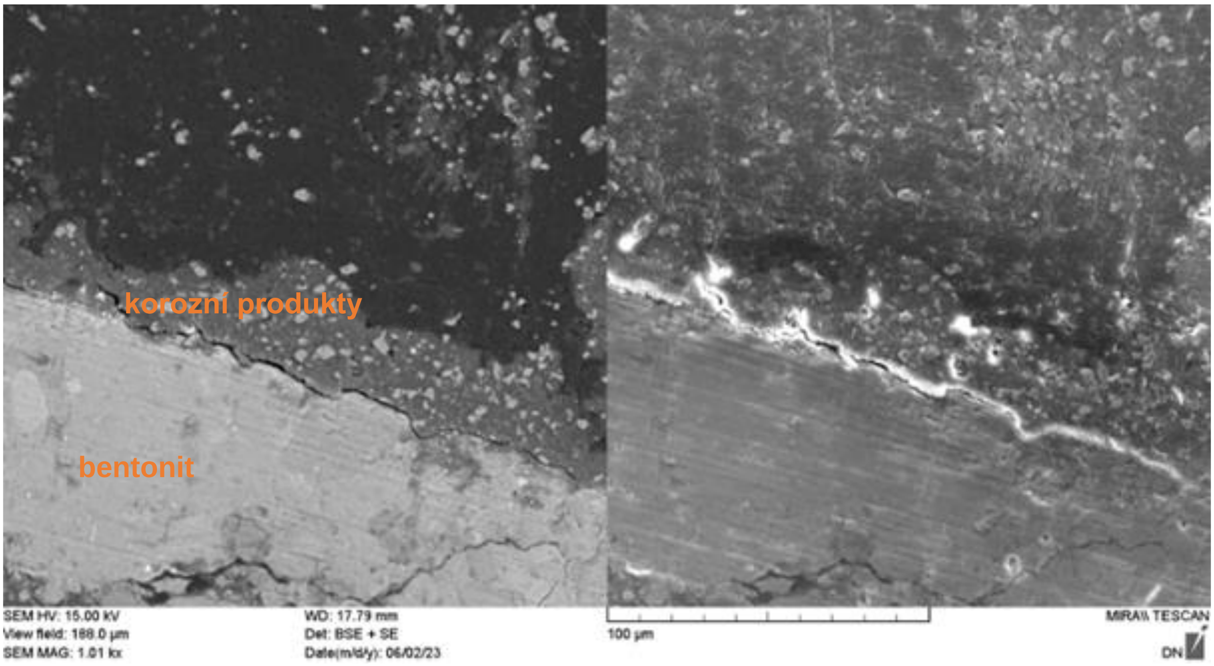

*Fig. 6 SEM images of the MaCoTe sample: BSE image on the left, SE image on the right*

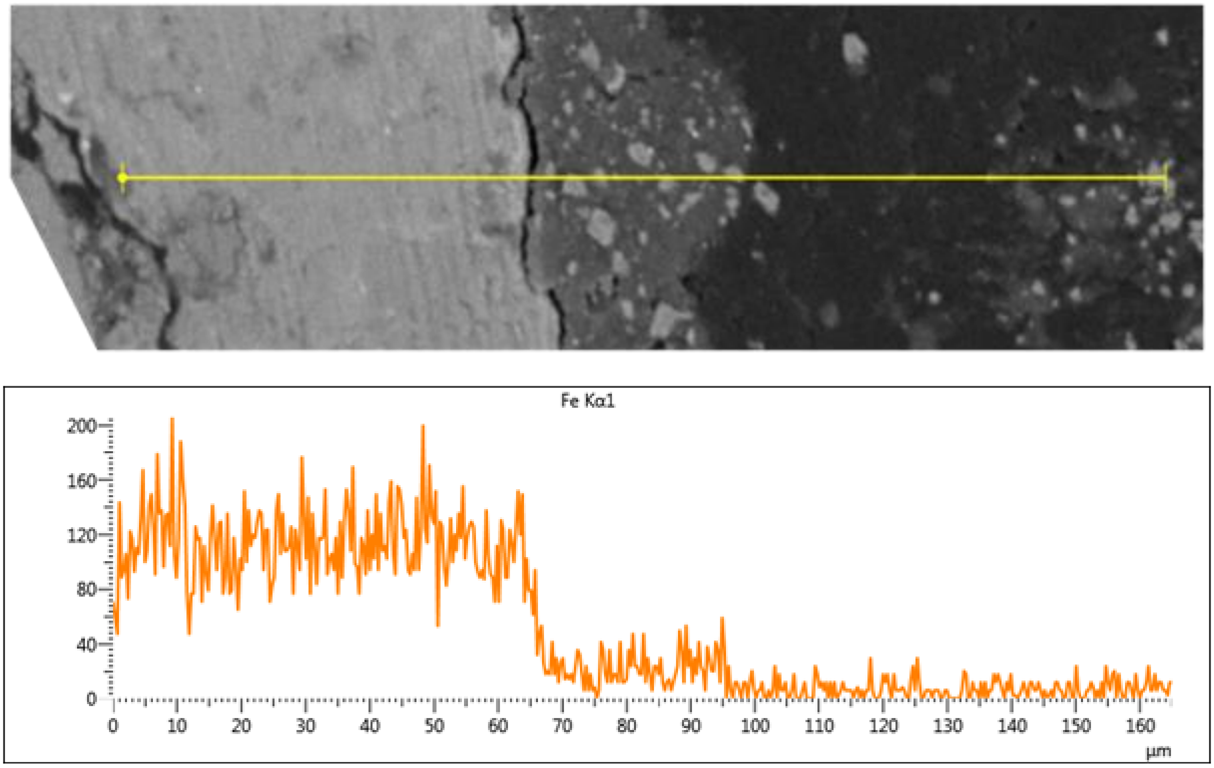

*Fig. 7 MaCoTe sample - line analysis of the Fe content: interface with the layer with the corrosion products*

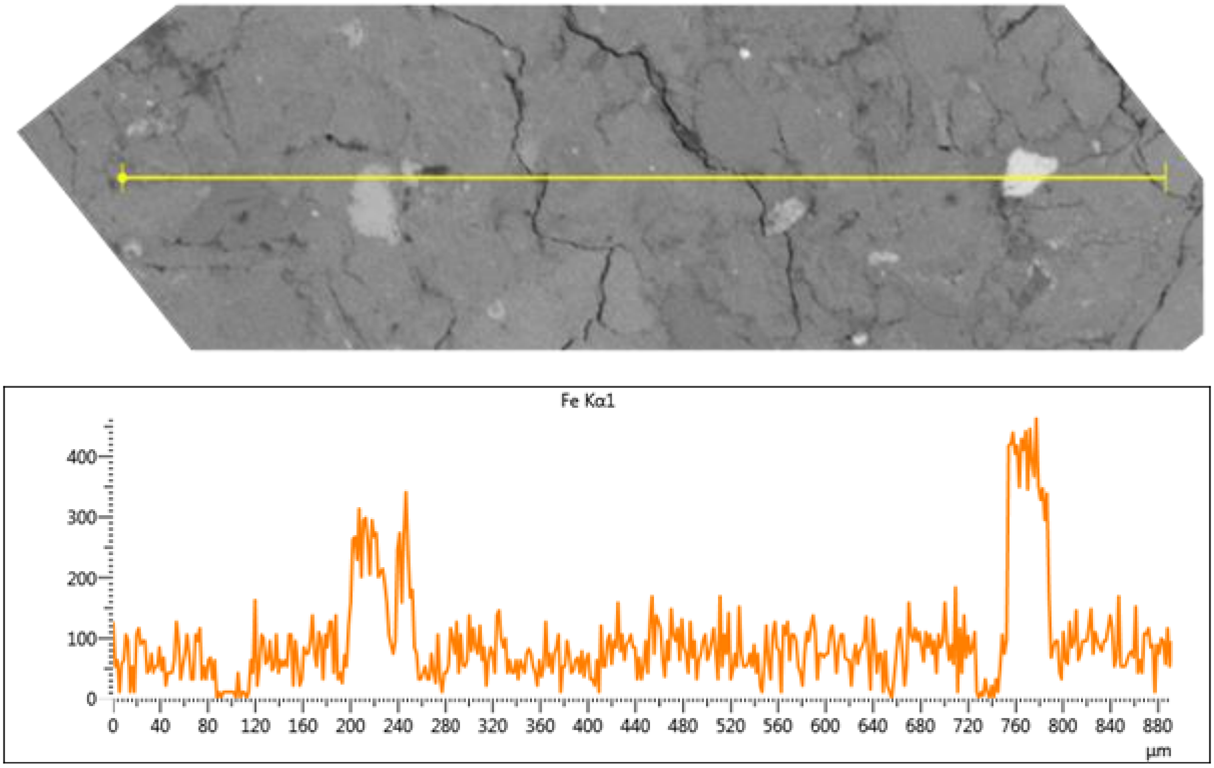

*Fig. 8 MaCoTe sample - line analysis of the Fe content: unaltered bentonite*

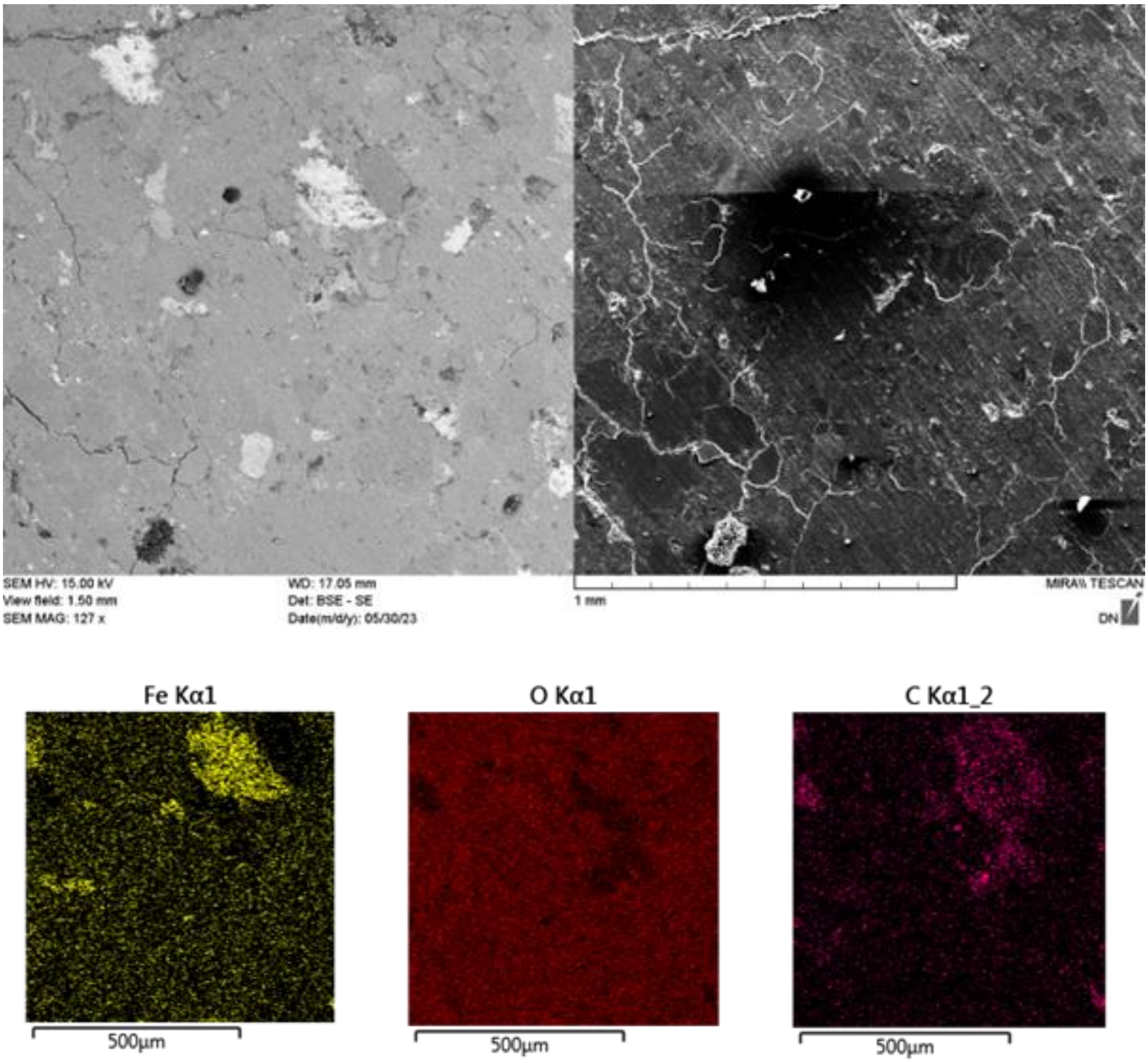

*Fig. 9 MaCoTe sample – EDS map: identification of higher density corrosion product particles (siderite)*

Both oxidic (Fig. 10, Fig. 16) and sulphide (Fig. 12, Fig. 14) iron ore particles were found to be present in the Kiruna A and B samples. The sulphide is most probably pyrite; its total volume fraction was below the XRD detection limit and, thus, it was not detected during the phase analysis. Fig. 11, Fig. 13, Fig. 15 and Fig. 17 serve to summarise the concentration gradient in the vicinity of the particles; again the gradient is very steep and, thus, does not indicate the precipitation of secondary corrosion products in the vicinity, nor the significant alteration of the clay.

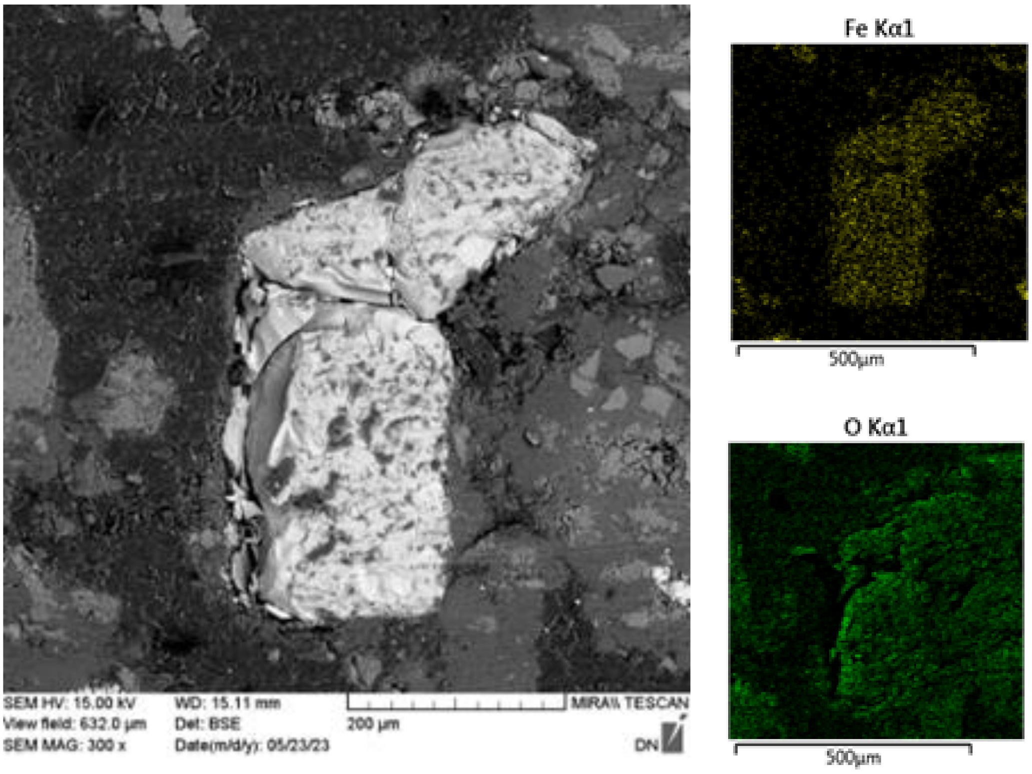

*Fig. 10 Kiruna sample A – EDS map: oxide particle*

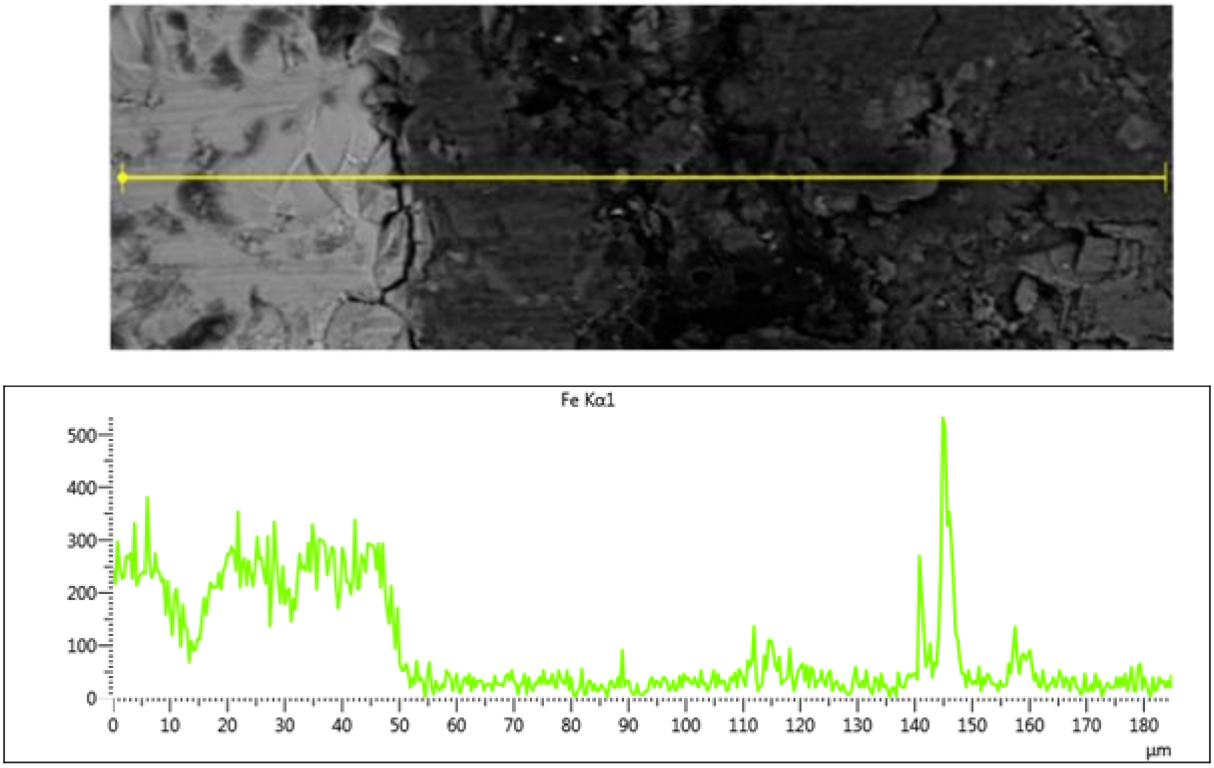

*Fig. 11 Kiruna sample A – line analysis of the Fe concentration: oxide particle - clay interface*

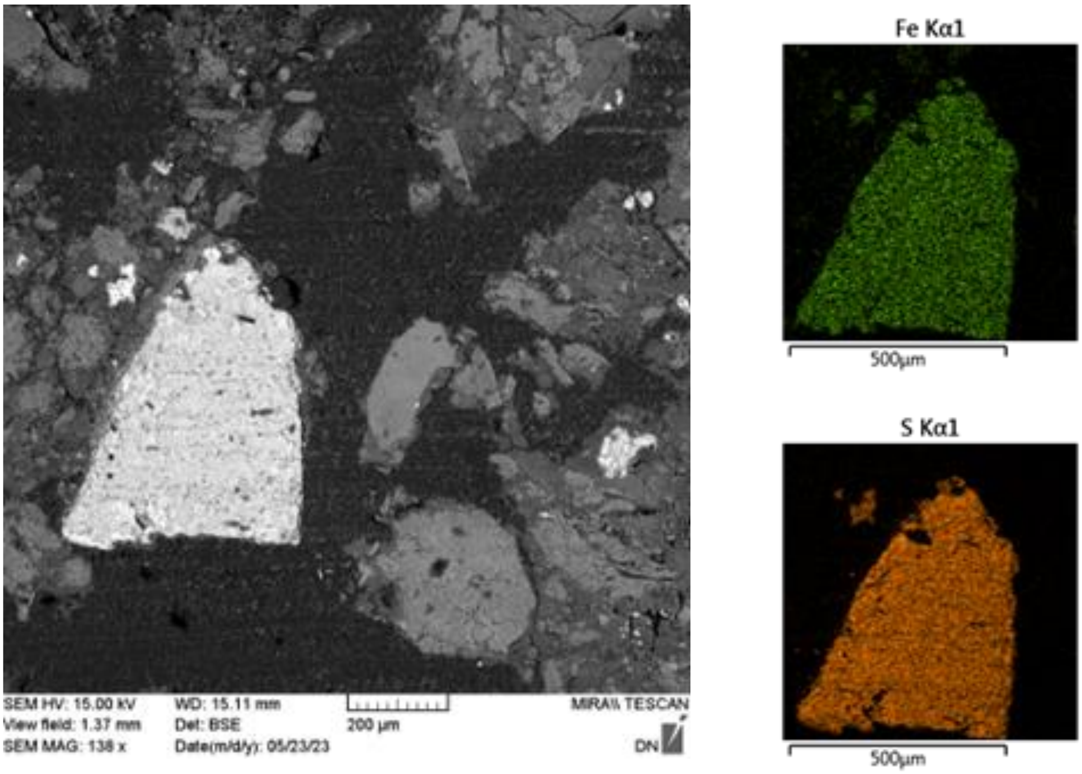

*Fig. 12 Kiruna sample A – EDS map: sulphide particle*

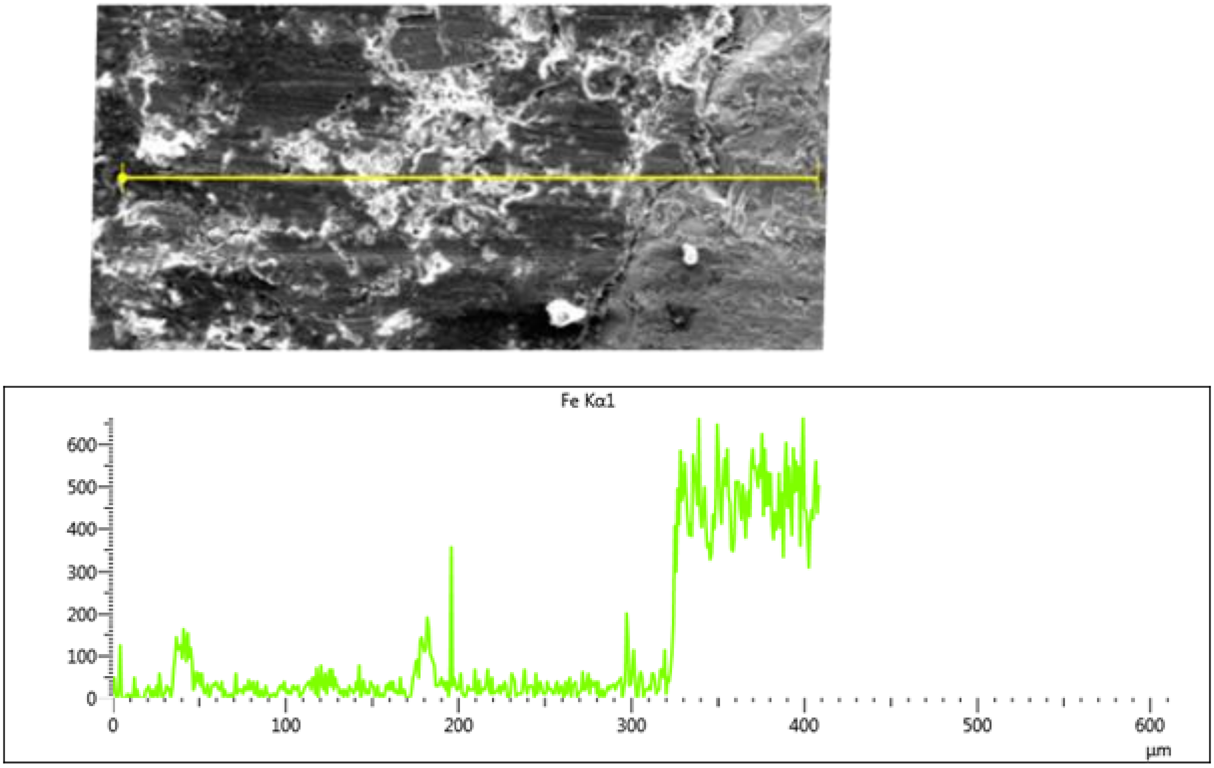

*Fig. 13 Kiruna sample A – line analysis of the Fe concentration: sulphide particle - clay interface*

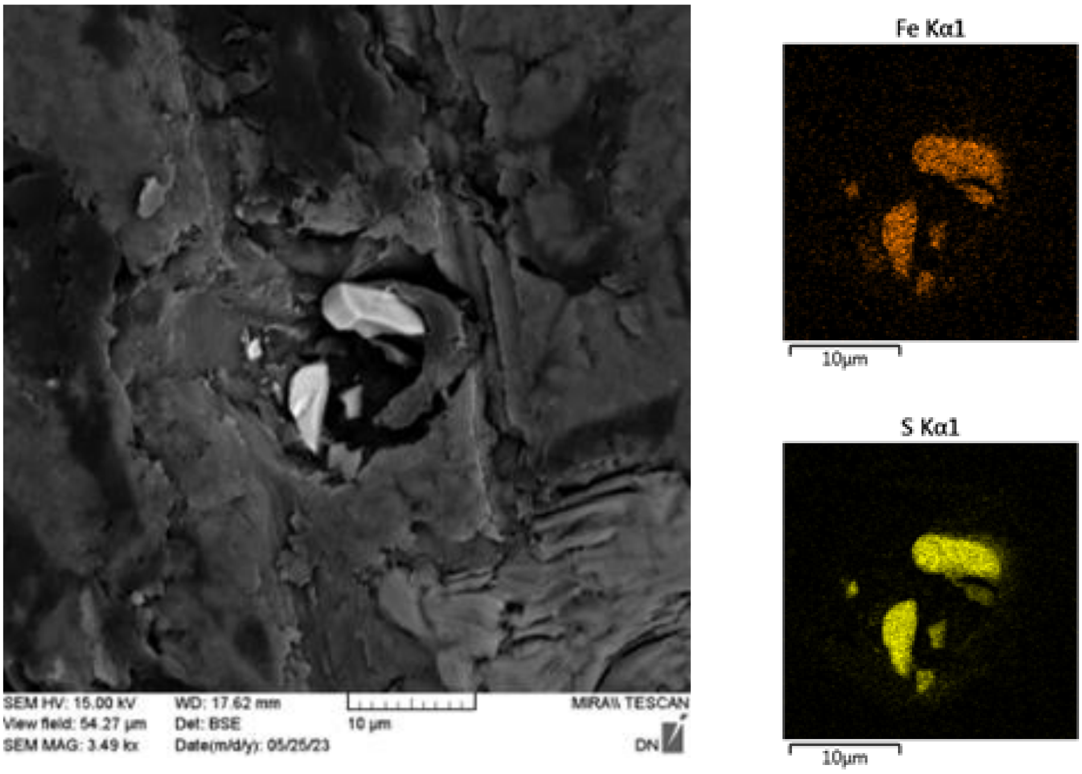

*Fig. 14 Kiruna sample B – EDS map: sulphide particle*

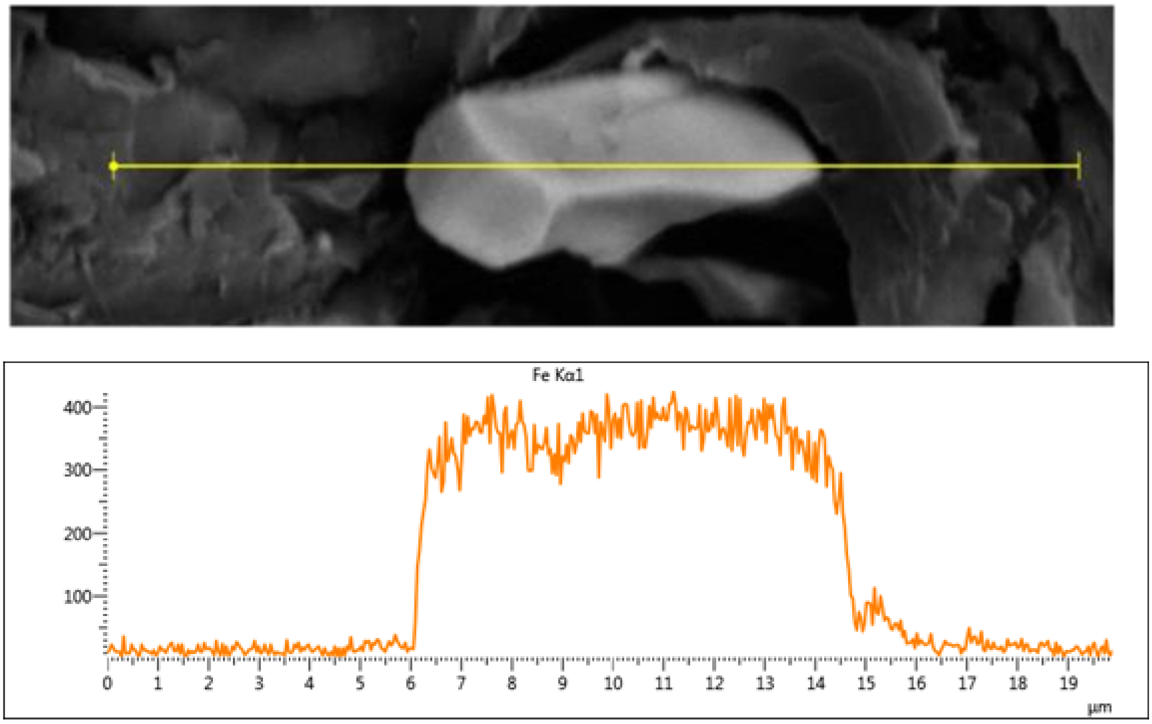

*Fig. 15 Kiruna sample B – line analysis of the Fe concentration: sulphide particle - clay interface*

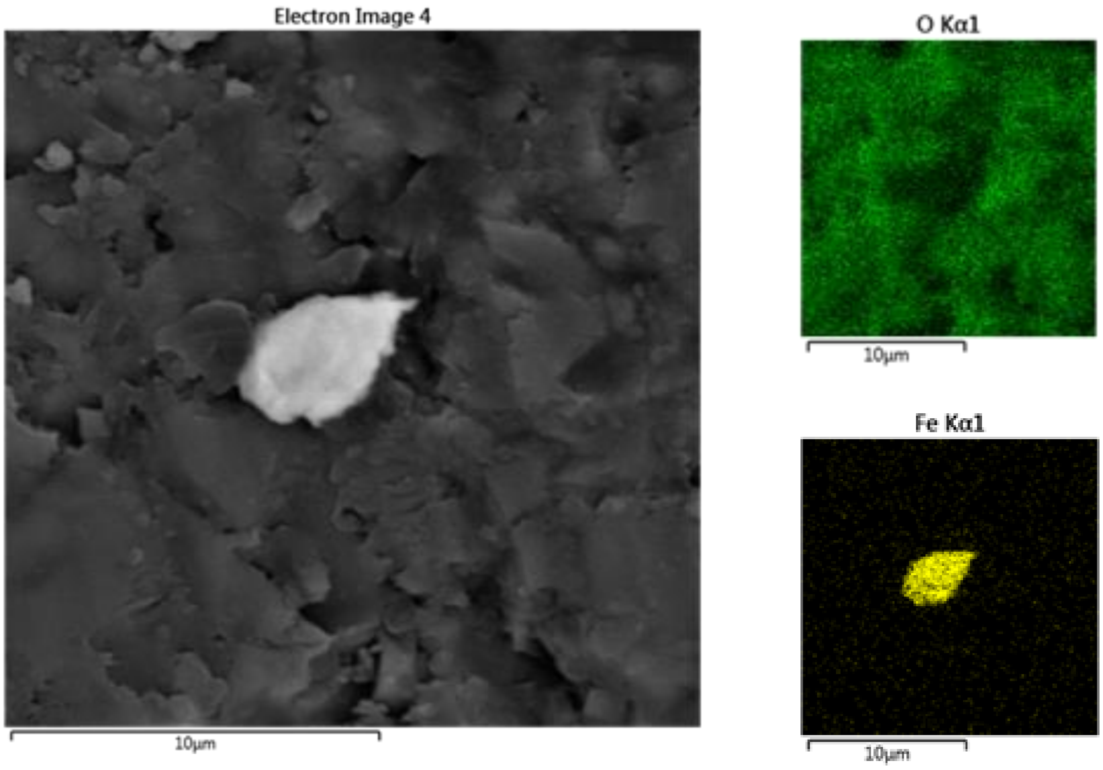

*Fig. 16 Kiruna sample B – EDS map: oxide particle*

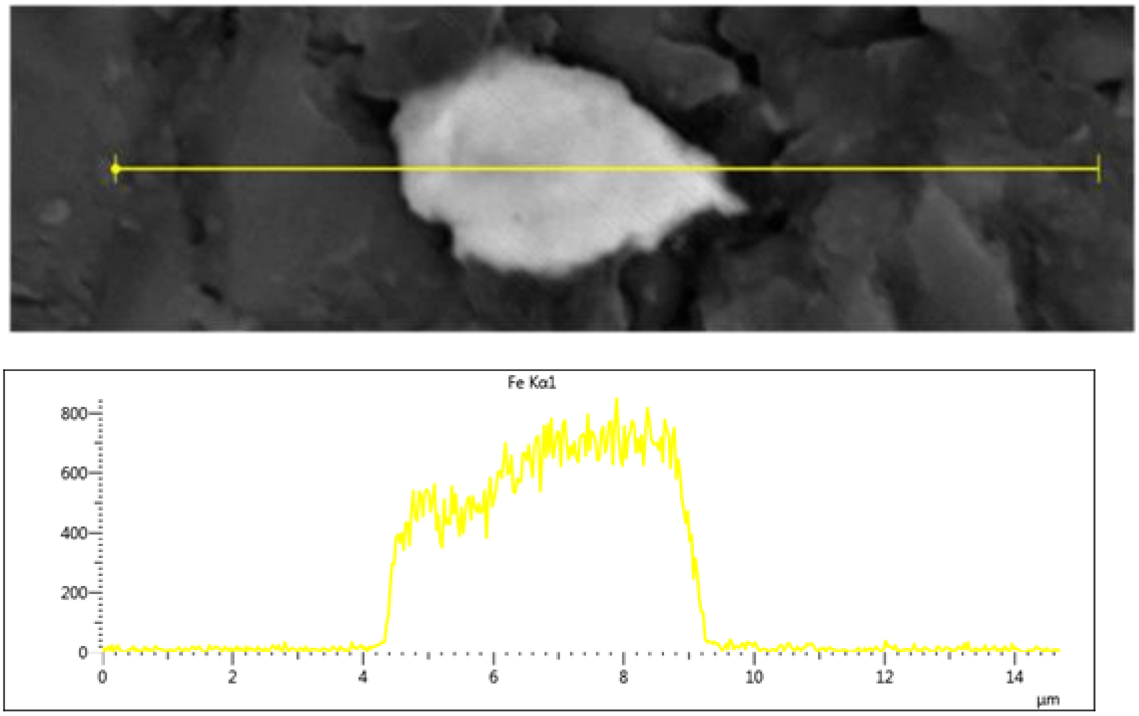

*Fig. 17 Kiruna sample B – line analysis of the Fe concentration: oxide particle - clay interface*

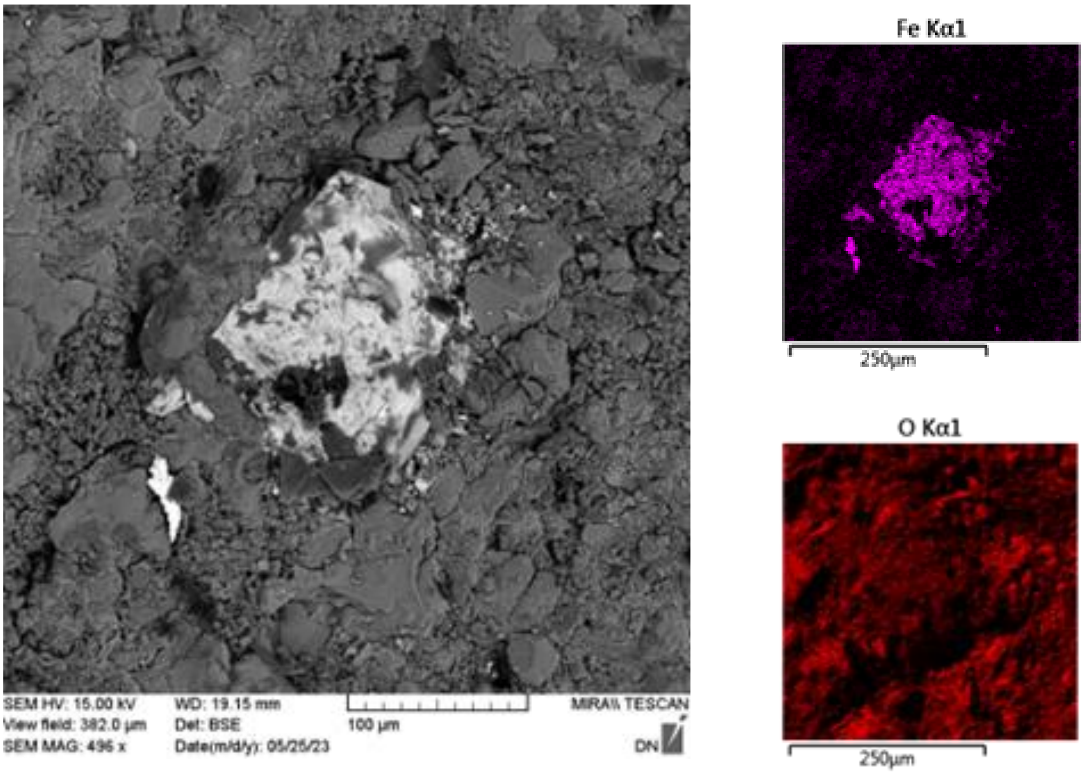

*Fig. 18 Kiruna sample C – EDS map: oxide particle*

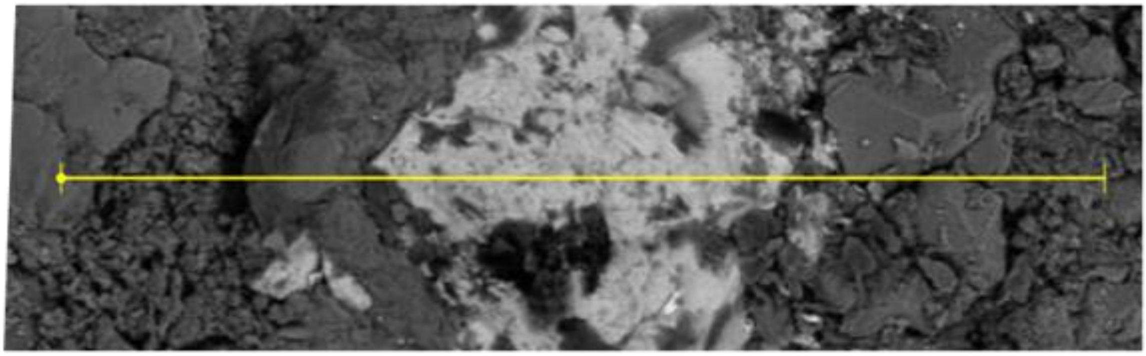

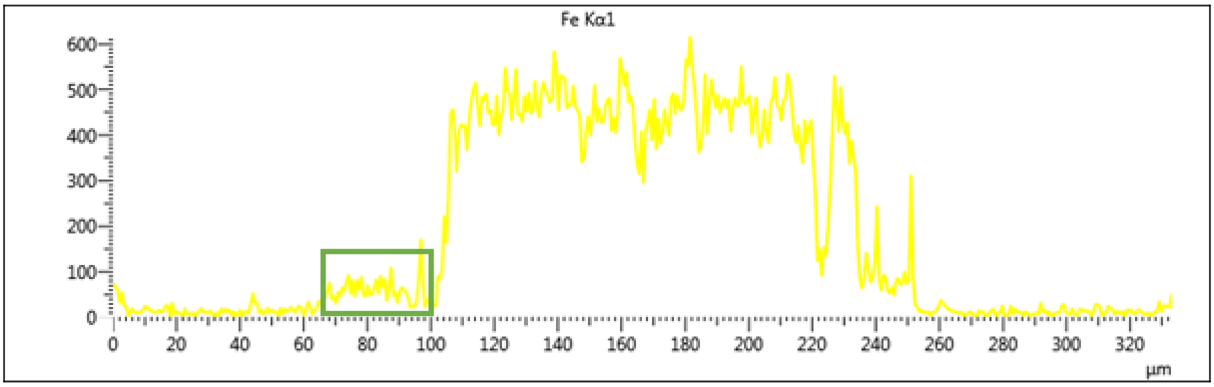

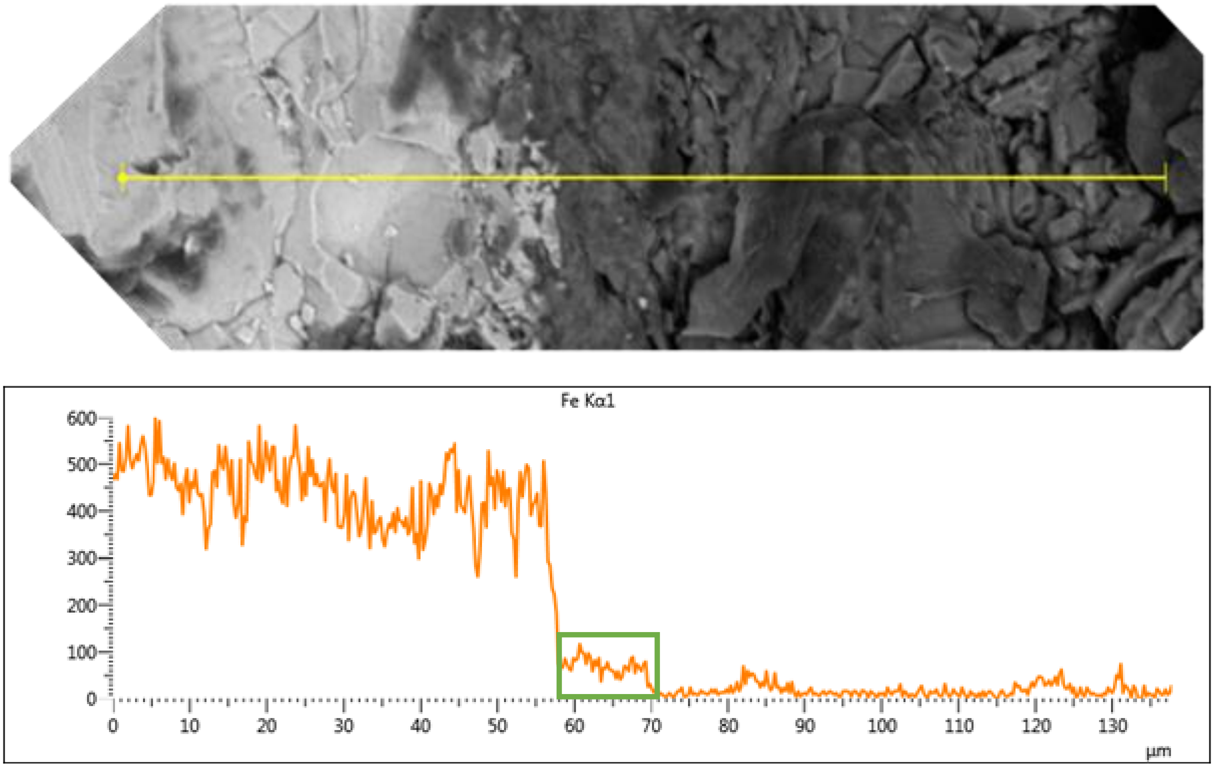

*Fig. 19 Kiruna sample C – line analysis of the Fe concentration: oxide particle - clay interface (above, the same particle as in Fig. 18, below, another particle in the same sample)*

Kiruna C sample contained only oxide particles (see Fig. 18). Areas of elevated Fe content in the clay in close proximity to the particle were found on the Kiruna C samples (Fig. 19). However, not all the particles were in the same locations nor were they continuous around the perimeter of a single particle. Thus, it cannot be stated with any certainty that the clay was significantly altered; rather, it suggests the presence of irregularities on the surface that were filled with clay and the emission of EDS signals from both phases.

# 4 Porosity

The porosity was determined using two techniques. First, the macroporosity was determined on the sanded samples employing the SEM method. Applying a magnification of 5000, the smallest visible pores were approximately 100 nm in size. Each image of the surface was thresholded and the pore area was determined relative to the total area of the images (see Fig. 20). Secondly, the microporosity was determined employing the BET method. Compacted oblong-shaped subsample weighing 1-2 g was extracted from each of the sample and emplaced in 10 mm-diameter test tube.

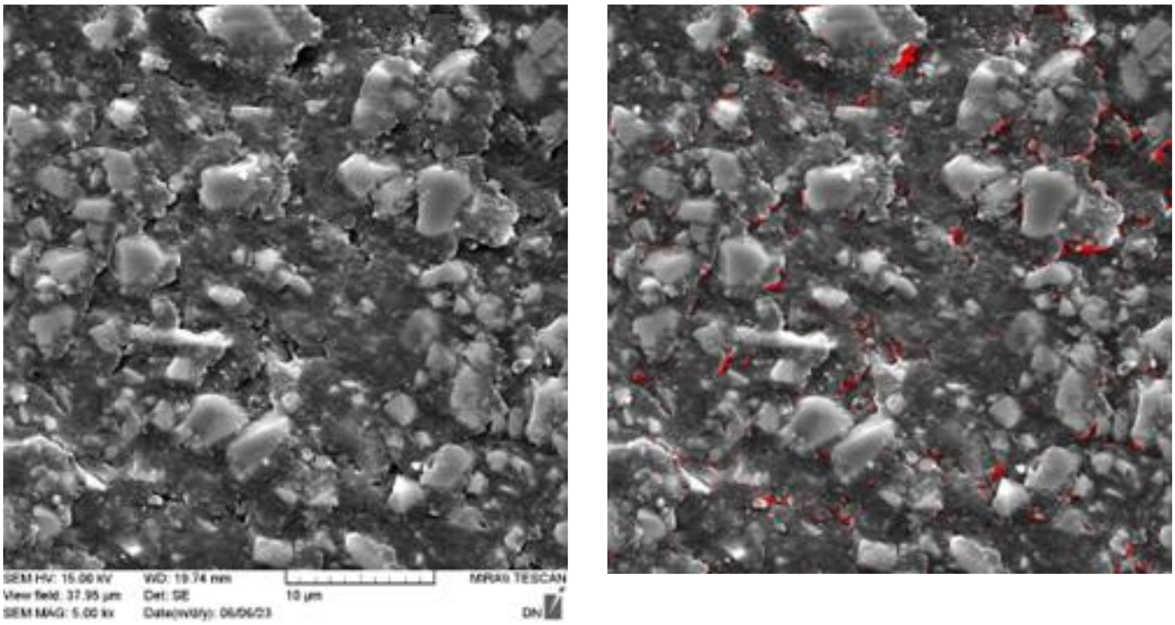

*Fig. 20 Thresholded images and the subtraction of the macropore area fraction (MockUp sample)*

The cumulative area fraction of the pores, which can also be considered to represent the volume fraction, is listed for all the samples in Tab. 3. The samples from Kiruna were found to contain significantly lower amounts of secondary phases than the MockUp and MaCoTe samples, which included a significant proportion of secondary corrosion products. The variance in the results was considerable with respect to all the sample types and was observed to be strongly dependent on the specific location on the sample. The macroporosities ranged from 0.1 vol.% and 5.8 vol.%. For comparison purposes, the macroporosity values of the samples studied in the Archaeological Analogues project (Stoulil et al. 2022) ranged from 2 vol.% to 7 vol.%.

The results of the microporosity measurements are shown in Tab. 4. The data for the Kiruna samples are merely indicative; it is uncertain whether the microporosity was affected by the precipitation of the secondary phases or by mechanical influences. Concerning the MaCoTe and MockUp samples, the results refer to the actual microporosity of the mixture of corrosion products and bentonite. The values are very high when one considers the original approximate porosity of the compacted bentonite, which for a dry density of 1500 kg.m$^{-3}$ would be at most 48 vol.%. However, the analysed corrosion products of the MaCoTe (34.6 vol.%) and MockUp

(27.8 vol.%) samples were still of only short-term duration in terms of the planned deep geological disposal period. For the sake of comparison, the microporosity of the long-term corrosion products of archaeological analogues was found to be significantly lower than for the MaCoTe and MockUp samples, ranging from 1 to 22 vol.%; moreover, the samples from 9 of the 15 analogue sites evinced microporosities within the narrow range of 15-18 vol.% (Stoulil et al. 2022).

*Tab. 3 Summary of the macroporosity measurement data*

| Sample/Macroporosity | Diameter | σ | MIN | MAX |
|---|---|---|---|---|
| Kiruna A | 0.012 | ± 0.007 | 0.003 | 0.027 |
| Kiruna B | 0.018 | ± 0.010 | 0.001 | 0.033 |
| Kiruna C | 0.009 | ± 0.010 | 0.001 | 0.035 |
| MaCoTe | 0.012 | ± 0.009 | 0.002 | 0.024 |
| MockUp | 0.025 | ± 0.021 | 0.003 | 0.058 |

*Tab. 4 Summary of the microporosity measurement data*

| Sample | Microporosity |
|---|---|
| Kiruna A | 0.012 |
| Kiruna B | 0.109 |
| Kiruna C | 0.083 |
| MaCoTe | 0.346 |
| MockUp | 0.278 |

# 5 Mechanical properties (nanoindentation)

Perpendicular sections of the samples embedded in epoxy resin and smoothed (see chapter 3) were subjected to nanoindentation testing. Details of these experiments can be found in Annex 2. Only a summary of the results of the measurement of the modulus of elasticity, which is the main quantity in terms of indicating the mechanical behaviour of corrosion product aggregates, is presented here.

The corrosion products of the MaCoTe sample (Fig. 21) behaved in a homogeneous manner from the interface to a depth of several micrometres into the layer of corrosion products. The average modulus of elasticity value was 3.3 GPa. With concern to the MockUp sample (Fig. 22), the outer part of the layer behaved differently, which was probably due to the higher degree of compaction of the material, the flow of the stiffening resin to a greater depth within the layer and/or the less complete contact of the indenter instrument with a sufficiently flat surface. The values determined at greater depths below the surface of the layer of corrosion products (around 4.3 GPa) were lower than those observed for the outer layer.

Correlation was determined between the microporosity and the modulus of elasticity (E) values. The layer with a higher porosity evinced a lower modulus of elasticity. The MaCoTe sample had a microporosity of 34.6 vol.% and E = 3.3 GPa; the MockUp sample had a microporosity of 27.8 vol.% and E = 4.3 GPa; and, for comparison purposes, archaeological analogues extracted from the Žehuň site (Stoulil et al. 2022) evinced a microporosity of 16 vol.% with an E in the range 8 – 52 GPa.

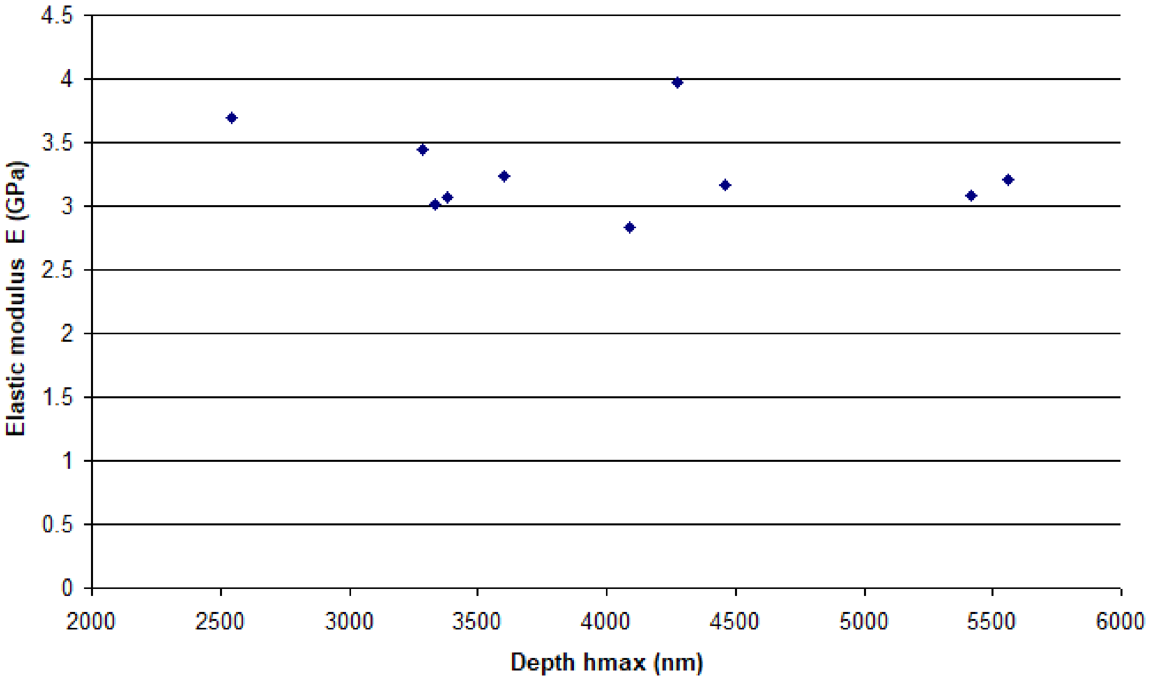

*Fig. 21 Results of the nanoindentation measurement of the modulus of elasticity of the corrosion products for the MaCoTe sample*

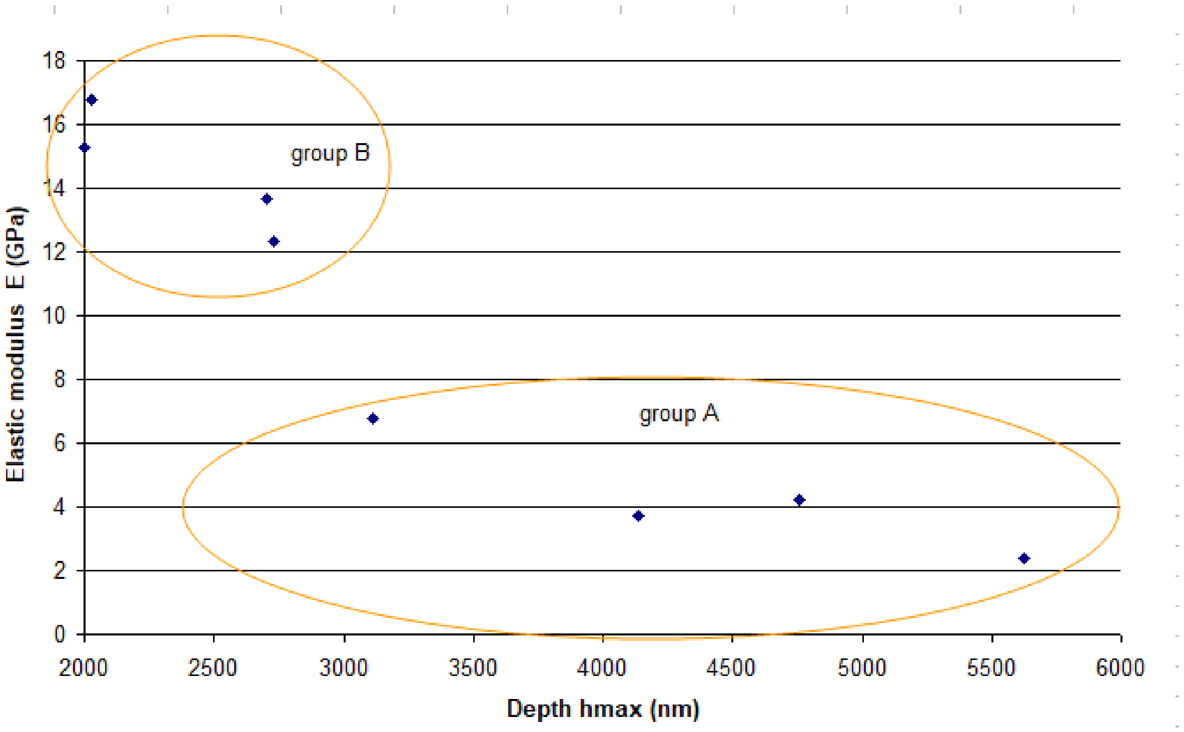

*Fig. 22 Results of the nanoindentation measurement of the modulus of elasticity of the corrosion products for the MockUp sample*

# 6 Conclusion

## Samples were analysed from two long-term experiments conducted under underground laboratory conditions along with three samples from the Kiruna mine in Sweden where particles of iron ore and smectite-rich clay have been in contact over the long term.

No secondary silicate phases with iron cations were detected in the Kiruna samples; moreover, not even the alteration of the clay around the particles was analytically demonstrable. Previous experimental observations of only the marginal and highly localised presence of silicate corrosion products over several years of laboratory experimentation (Forman et al. 2021), as well as the undeterminable amount of silicate corrosion products in archaeological analogues after at least several hundred years of exposure (Stoulil et al. 2022), are consistent with the results obtained for the Kiruna samples, which had been exposed for at least hundreds of millions of years. Thus, it is unnecessary to take into account (alumino)silicate phases in deep geological repository lifespan models.

Siderite was observed to be the main corrosion product in the MaCoTe and MockUp samples. Even taking into consideration that these experiments have been underway for several years, the contact period is still relatively short-term, and the corrosion products are still mixed with the bentonite particles. Although the alteration of the bentonite by iron cations was visually identifiable, the iron content was still below the detection capability of the SEM/EDS method. For the same reason, i.e., the short-term exposure period, the corrosion products have not yet been completely sealed and evince high microporosity values, which directly impacts the mechanical properties, as represented in this study by the modulus of elasticity. However, with concern to the use of models in the ongoing Safety 2 project, it will be necessary to verify the data on the mechanical properties of siderite employing more compact samples of the pure mineral and simulated laboratory samples.

## References

FORMAN L. a kol. (2021) Závěrečná technická zpráva výzkumná část projektu Výzkum a vývoj ukládacího obalového souboru pro hlubinné ukládání vyhořelého jaderného paliva do stadia realizace vzorku. ZZ SÚRAO 544/2021.

GILG H. A. a ANDERSSON U. B. (2020) Geology of deep clay alteration zones in the Kiirunavaara and other iron ore deposits, northern Norrbotten, Sweden. Nagra Report.

GONDOLLI J. a kol. (2018) Korozní produkty – závěrečná zpráva. TZ SÚRAO 329/2018.

STOULIL J. a kol. (2022) Archeologické analogy pro verifikaci modelů životnosti kontejneru pro hlubinná úložiště radioaktivního odpadu. TZ SÚRAO 623/2022.

ZUNA M. a kol. (2023): Korozní zkouška v přírodním granitoidním prostředí – zapojení v projektu Material Corrosion Test (MaCoTe), část zakázky č. 2 realizace a vyhodnocení MaCoTe experimentu v Grimsel Test Site, TZ SÚRAO.

SÚRAO
SPRÁVA ÚLOŽIŠŤ
RADIOAKTIVNÍCH
ODPADŮ

NAŠE
BEZPEČNÁ
BUDOUCNOST

**www.surao.cz**